Received: 31 December 2020 | Revised: 9 April 2021 | Accepted: 24 April 2021

High Voltage

DOI: 10.1049/hve2.12111

国家电网 STATE GRID 中国电力科学研究院有限公司 CHINA ELECTRIC POWER RESEARCH INSTITUTE

The Institution of Engineering and Technology

WILEY

ORIGINAL RESEARCH PAPER

Oxidative modifications and structural changes of human serum albumin in response to air dielectric barrier discharge plasma

Siqi Peng[1] | Liyang Zhang[1] | Dongheyu Zhang[1] | Yuntao Guo[1] | Xinxin Wang[1] | Qun Zhou[2] | Haiyun Luo[1]

[1]Department of Electrical Engineering, Tsinghua University, Beijing, China

[2]Department of Chemistry, Key Laboratory of Bioorganic Phosphorus Chemistry and Chemical Biology (Ministry of Education), Tsinghua University, Beijing, China

Correspondence

Qun Zhou, Department of Chemistry, Key Laboratory of Bioorganic Phosphorus Chemistry and Chemical Biology (Ministry of Education), Tsinghua University, Beijing, China.
E-mail: zhouqun@tsinghua.edu.cn

Haiyun Luo, Department of Electrical Engineering, Tsinghua University, Beijing 100084, China.
Email: lhy@tsinghua.edu.cn

Associate Editor: Dunpin Hong

Funding information

National Natural Science Foundation of China, Grant/Award Number: 52041701; Tsinghua University-Peking Union Medical College Hospital Initiative Scientific Research Programme, Grant/Award Number: 20191080604; Tsinghua University Spring Breeze Fund, Grant/Award Number: 2020Z99CFG007

Abstract

In this work, the air dielectric barrier discharge plasma was applied to a model of protein human serum albumin to explore plasma-mediated protein damage from a biomolecular perspective. Carbonylation and side chain modifications of protein in solution were observed by Fourier transform infrared (FT-IR) spectroscopy and mass spectrometry (MS). Protein backbone cleavage is proved by Bradford assay, sodium dodecyl sulphate–polyacrylamide gel electrophoresis, and MS. Typical fragments are in the range of 10–12 kDa. The decrease in α-helix and increase in β-sheet indicated by FT-IR are major protein secondary structure changes. Accordingly, a whole map of protein oxidative damage and structural changes in response to the plasma was postulated.

1 | INTRODUCTION

Low-temperature plasma (LTP) has drawn increasing attention for broad biological and medical applications, including research topics of microbiological inactivation, wound healing, selective cancer treatment, and plasma stomatology [1–4]. The main attraction is that LTP can produce a chemically enriched environment containing various reactive oxygen and/or nitrogen species (RONS) at close to room temperature, by gaseous transport or plasma–liquid interactions [5, 6]. Yet it remains incompletely understood how biological targets respond to RONS produced by LTP.

As the basic unit of all living biological objects, protein has drawn a lot of interest. Earlier studies used plasma for protein decontamination [7–9]. Contaminated protein can be efficiently removed from surfaces by plasma, reducing the risk for potential transmissible infections. In addition, protein oxidative damage is closely related to LTP-based bacterial inactivation [10, 11]. For instance, membrane protein modification is postulated to be the major cause of bacterial death [10]. Protein in solution responds to plasma in a totally different manner than that in a dried state, possibly owing to the intrinsically more complex physical and chemical processes [12]. When the solution is exposed to the plasma, short-lived species (i.e., $\cdot OH$, $ONOO^-$) and long-lived species (H_2O_2, NO_2^-, and NO_3^-) are produced. It is worth investigating the exact responses of proteins to plasma exposure and the underlying molecular mechanisms.

The validated effects of plasma on proteins in solution can be roughly divided into two categories: oxidative modifications and the structural changes. Protein oxidation by plasma involves

the modification of amino acid side chains [13–16], carbonylation [13, 15, 17], and disulfide bond cross-links [12, 13, 18, 19]. The most pronounced side chain modifications involve the sulphonation of free sulfhydryl groups, which is also observed in treated amino acid solutions [20]. Protein carbonylation is a commonly used indicator of protein oxidation. The formation of carbonyls is postulated to arise from modifications of –NH or –NH_2 containing an amino acid side chain or peptide bond cleavage [13]. Protein oxidation by plasma acts similarly to that in life science, through ageing, oxidative stress, and some pathological conditions [21].

With respect to protein primary structure changes, although dielectric barrier discharge (DBD) or plasma jet does not necessarily lead to protein degradation [12, 22], several have proved the cleavage of peptide bond of proteins induced by plasma [17, 23–25]. Consequently, it is still unclear whether the RONS affects protein cleaving into fragments. Regarding a secondary structure, it is generally discovered that plasma can induce a decrease in α-helix/β-turn structures and an increase in β-sheet/random-coil contents in polyphenoloxidase and peroxidase [26], myofibrillar protein [15], myoglobin [27], and bacterial membrane/intracellular proteins [10].

Various analytical techniques were applied to gain more comprehensive insights into human serum albumin (HSA) injuries induced by air DBD plasma. Protein backbone cleavage by plasma was measured by denaturing sodium dodecyl sulphate–polyacrylamide gel electrophoresis (SDS-PAGE) and matrix-assisted laser desorption-ionization time of flight mass spectrometry (MALDI-TOF MS). Liquid chromatography (LC)—electrospray ionization ion trap (ESI-IT) MS was applied to study oxidative responses to plasma. Findings obtained by these techniques were also confirmed by Fourier transform infrared (FT-IR) spectroscopy, which is regarded as a powerful tool to evaluate both biological and nonbiological material modifications [11, 28]. We intend to give a whole map for how proteins in liquid respond to air plasma, which is necessary to reveal the mechanisms of interactions between plasma and living cells, thus facilitating the relevant applications.

2 | MATERIALS AND METHODS

2.1 | Sample preparation and plasma treatment

The standard HSA solution with a concentration of 5% (w/v) was bought from Shanghai Yuanye Bio-Technology Co., Ltd. First, the solution was diluted with deionised water to 25 mg/mL, which is the optimal concentration for FT-IR analysis. After that, 5 μL of the solution was transferred onto a calcium fluoride (CaF_2) window as one sample waiting for plasma treatment. Each sample was immediately exposed to the air plasma for different times (0, 2, 4, 6 and 8 min). After treatment, the drop after drying under room temperature was subjected to FT-IR measurements or was washed by 100-μL deionised water and transferred to an Eppendorf tube for other tests.

The plane DBD configuration is shown in Figure 1. Electrodes were made of aluminium with a diameter of 50 mm. A hollow acrylic glass chamber of 100 × 80 × 9 mm with an internal space of 98 × 70 × 3 mm was clamped between electrodes. When exposing the HSA sample to plasma, the CaF_2 window was placed inside the poly(methyl methacrylate) chamber and kept in the centre of the electrodes. In our experiment, the CaF_2 window was 13 mm in diameter and 1 mm thick, which fixed the thickness of air plasma at 2 mm. The two electrodes were connected to an AC high voltage source bought from Nanjing Suman Co. Ltd. The peak voltage was 16 kV and the frequency was 1.5 kHz. The average discharge power was calculated to be approximately 4 W. The air DBD plasma was photographed by an EOS M2 Canon camera with an exposure time of 5 s, an F value of 5.6 and an ISO of 200, whereas the voltage and current were measured using a high-voltage probe (P6015 A, Tektronix) and a current probe (TCP312 A, Tektronix), respectively. Plasma was successfully generated between the electrodes, shown as a dashed line area in Figure 1a, especially upon the CaF_2 window. As long as the applied voltage was not too high, the plasma would keep steady without obvious filaments or sparks. To obtain the gas temperature of DBD by optical emission spectroscopy, a spectrometer (Princeton Instrument Acton SpectraPro 2500i) was used to get the spectrum (Figure S1).

2.2 | Fourier transform infrared measurements

The dried sample was measured by a 5X beam condenser accessory equipped in a Perkin-Elmer infrared spectrometer with a resolution of 4 cm^{-1}. The infrared spectra were collected from 4000 to 900 cm^{-1} with 16 scans. All raw spectral data were preprocessed with baseline correction on the PerkinElmer Spectrum (version 10.5.4). For further analysis, spectra in the range of 4000–2000 cm^{-1} and 2500–900 cm^{-1} were separately normalized to the amide A (~3200 cm^{-1}) and amide I band, respectively. The amide I band was subjected to baseline correction and fitted by Gaussian curves to obtain the contents of the contained protein secondary structures [19, 29, 30]. The initial band locations of secondary structure components were determined by second derivative infrared spectra. The results of curve fitting deconvolution with the goodness of fit (r^2) were greater than 0.99.

2.3 | Matrix-assisted laser desorption-ionization time of flight and liquid chromatography ion trap/time of flight mass spectrometry

Mass spectra of the untreated and treated protein solution were recorded by a MALDI-TOF mass spectrometer (AXIMA-Performance MA) in the range of 100–800,000 m/z. The compound sinapinic acid was used as the matrix and mixed with the protein sample before exposure to the laser. The whole mass spectrum was divided into four ranges (100–3000,

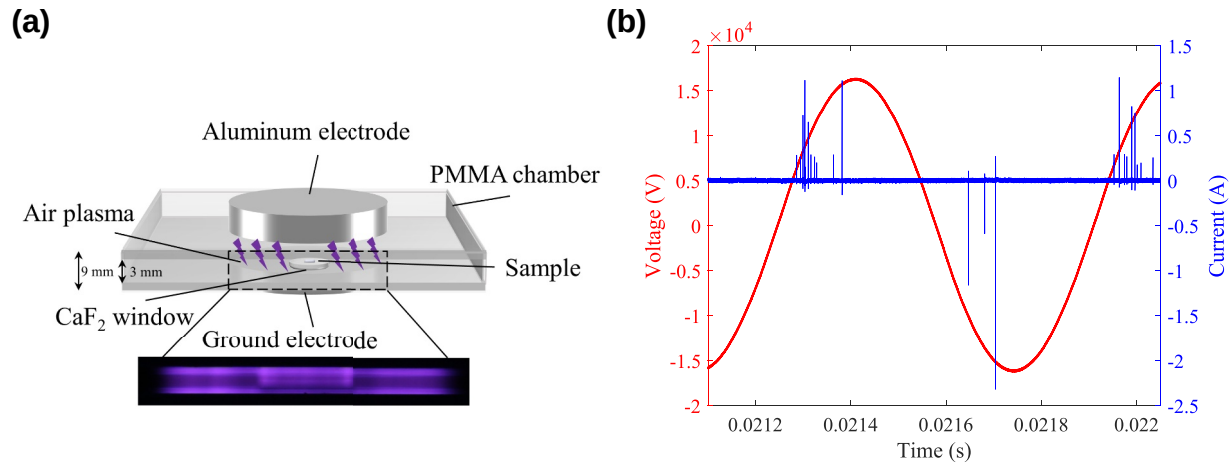

FIGURE 1 Dielectric barrier discharge (DBD) setup and electrical parameters. (a) Schematic diagram of DBD configuration and photograph of filamentary discharge. The total air gap is 3 mm. The thickness and diameter of the CaF_2 window are 1 and 13 mm, respectively. The exposure time, F value and ISO of the discharge photograph are 5 s, 5.6 and 200, respectively. (b) Waveforms of discharge voltage and current

1000–10,000, 10,000–30,000, and 30,000–80,000 m/z), which required different input laser energies to optimise ionization efficiency. The potential protein fragments after treatment can be identified when keeping the same input laser energy for all samples in each scan range.

To clarify the side chain modifications of HSA by plasma, the cysteine and methionine were dissolved in deionized water to the concentration of 25 mg/mL and then treated in the same condition as in Section 2.1. The mass spectra in the range of 50–500 m/z were collected by an LC ESI-IT/TOF MS (Shimadzu. Japan) at positive-ion mode using 10% acetonitrile plus 90% water as the eluent.

2.4 | Sodium dodecyl sulphate–polyacrylamide gel electrophoresis

The SDS-PAGE Gel Kit, 4× loading buffer, and protein marker (14.4-97.4 kD) were purchased from Solarbio (Beijing, China). The treated protein solution (30 μL) was mixed with the 4× loading buffer and incubated at 100°C for 5 min. The final loading capacity for each sample was 20 μL. The gels were run at 100 V for 30 min and subsequently at 150 V for 1 h. Then, the gels were stained with the M5 HiPer gel staining solution (Mei5bio) and photographed with the gel imaging system (GenoSens2100, Clinx Science Instruments Co., Ltd.). Primary structural changes of HSA before and after treatment can be inspected by the final stained bands.

2.5 | Bradford assay

The protein solution was first diluted three times with deionised water. The concentration of the protein was quantified by Bradford assay using a commercially available kit (Bradford Protein Assay Kit, Solarbio) according to the manufacturer's instructions. Briefly, a 20-μL protein sample and 200-μL 1× G250 dye solution were added to 96-well plates and allowed to react for 5 min. Afterwards, absorbance at 595 nm of the solution was recorded by a microplate reader (SpectraMax i3x, Molecular Devices). The protein concentration was obtained from the standard absorption curve of the HSA standard.

2.6 | Spectrophotometric protein carbonyl assay

Protein carbonylation was quantified by the 2,4-dinitrophenylhydrazine(DNPH) assay using a Protein Carbonyl Colourimetric Assay Kit (Solarbio). The procedures can also be found in Wehr and Levine [31]. Absorbance at 370 nm of the final solution was measured by the microplate reader and used to calculate the carbonyl content.

3 | RESULTS AND DISCUSSION

3.1 | Protein carbonylation, side chain modifications and cross-linking

The appearance of the treated protein samples becomes cloudier and even pale yellow with plasma treatment (Figure S2), which is related to modifications or destruction of the chromophores in the protein. The infrared spectra are shown in Figure 2, where significant spectral variations are observed. The assignments of the major bands are shown in Table 1 [32, 33].

The carbonyl contents of the control and 8-min–treated samples are 1.93 and 30.31 nmol/mg, respectively, as determined by DNPH assay. The increase in carbonyl groups is also proved by the infrared spectra, in which the newly generated shoulder representing the stretches of C=O at ~1725 cm^{-1} increases sharply with treatment time.

The side chain modifications induced by plasma could be observed in the infrared spectra. As in Figure 2, the peak

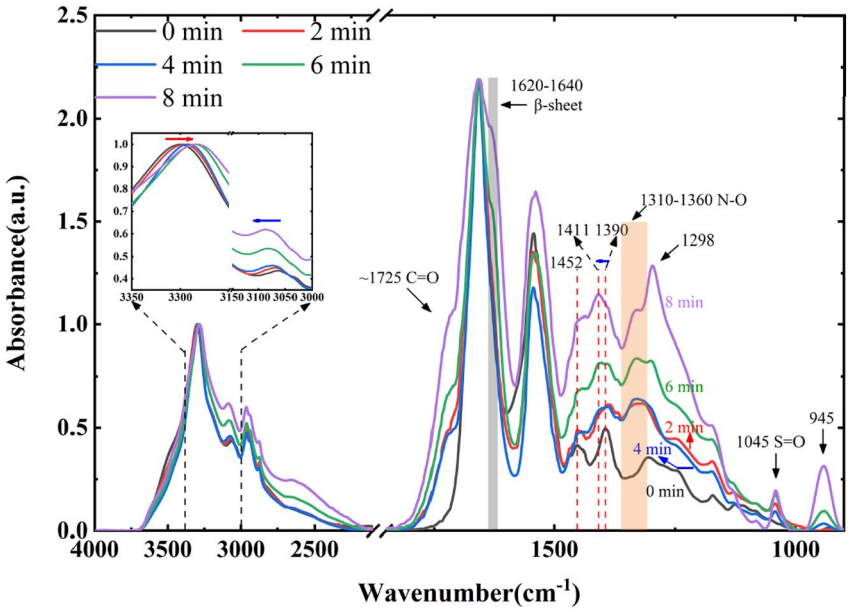

FIGURE 2 Fourier transform infrared spectra of human serum albumin samples with plasma treatment times of 0, 2, 4, 6, and 8 min

TABLE 1 Bands assignments of infrared spectra [32, 33]

Wavenumber (cm^{-1})	Assignments
1600–1695	Amide I (C=O stretch)
~1725	C=O stretch
1480–1575	Amide II (C-N stretch; N-H bend.)
1360	N-O str.
1220–1320	Amide III (C-N stretch; N-H bend.)
1045	S=O sym. str.

Abbreviation: sym, symmetric.

at 1315–1360 cm^{-1} denoting stretching of N-O increases after treatment, which is also found in the plasma-treated water (Figure S3). Consequently, this peak is most possibly from reactive nitrogen species such as nitrite and nitric acids. The new sharp peak at 1045 cm^{-1}, shown as S=O, stretches from the oxidation products of sulphur amino acids such as cysteine and methionine. These products can be identified by ESI MS using amino acids as the treatment targets. According to Figure 3a, the $(Cys)H^+$ at 122.03 *m/z* in the control group is oxidised to $(Cys+3O)H^+$ at 170.01 and $(2Cys\text{-}2H)H^+$ at 241.03 (*m/z*) after 8 min treatment. The product $(Cys+3O)H^+$ denotes the formation of sulfonic acids, whereas the $(2Cys\text{-}2H)H^+$ is caused by the cross-link of two cysteines through a disulfide bond [20]. The peaks at 150.06, 133.03 and 172.04 m/z in the Met control are from $(Met)H^+$, $(Met\text{-}NH_3)H^+$ and $(M\text{-}et)Na^+$, respectively (Figure 3b). After 8 min treatment, the intermediate oxidation products $(Met + O\text{-}CH_3SOH)H^+$, $(Met+2O\text{-}CH_3SOH)H^+$, $(Met + O)H^+$ and $(Met+2O)H^+$ at 102.03, 118.05, 166.05 and 182.04 *m/z*, as well as final products $(Met\text{-}2H+3O\text{-}C)H^+$ and $(Met+2O\text{-}CO\text{-}H_2O)H^+$ at 184.01 and 136.06 *m/z*, are produced [20]. The MS results of free amino acid modifications are also applicable to proteins, which is consistent with the FT-IR results.

3.2 | Primary structure changes

The primary structure alterations of HSA before and after plasma treatment are first examined by Bradford assay. This assay is based on the binding of Coomassie brilliant blue dye to the proteins through Van der Waals forces and hydrophobic interactions [34]. As is in Figure 4a, the protein concentration decreases with treatment time. After treatment for 6 min, the protein concentration is close to the detection limit, suggesting the complete destruction of protein structures. A similar study by Krewing et al. showed that the protein concentration decreased by 50% after plasma treatment for 10 min under AC high voltage at 300 Hz [23]. In Figure 4a, a close result was obtained after 2 min treatment at 1.5 kHz alternating high voltage.

Direct evidence of a protein backbone cleavage is provided by the SDS-PAGE results. As in the electrophoresis image shown in Figure 4b, the lanes from left to right correspond to the protein marker, untreated and treated samples (2, 4, 6 and 8 min), respectively. The bands of HSA become increasingly weaker along with the treatment time, indicating gradual peptide backbone cleavage into fragments less than 20 kDa.

To validate these experimental results and obtain more detailed information on protein fragmentation, the control and treated samples were examined by MALDI-TOF MS analysis. The signal of intact HSA at ~66000 m/z significantly decreases after treatment, almost diminishing at 4 and 8 min (Figure 5d).

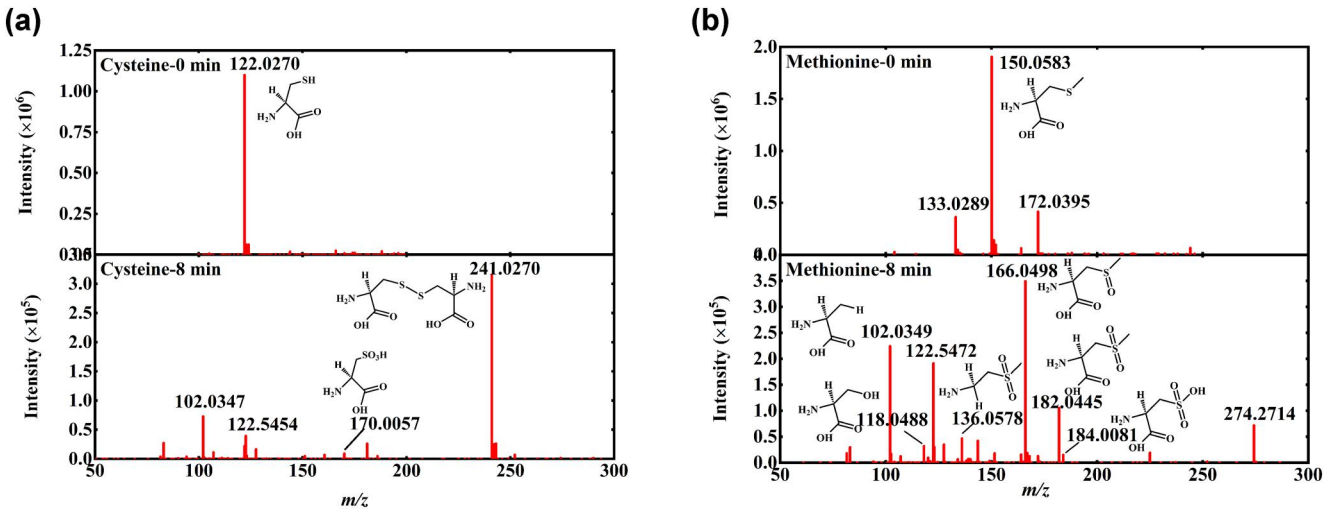

FIGURE 3 Electrospray ionization mass spectrometry spectra of amino acids before and after plasma treatment (a) cysteine, (b) methionine

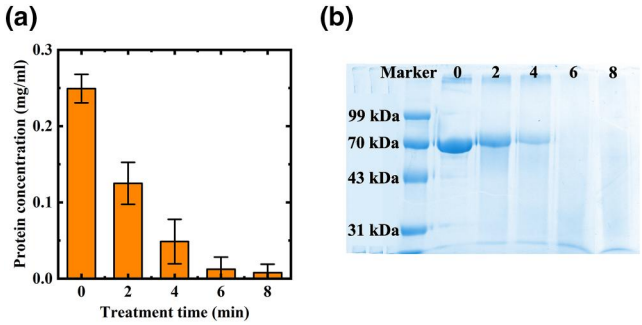

FIGURE 4 Protein concentration and molecular weight of samples. (a) Human serum albumin (HSA) concentration measured by Bradford assay with respect to different plasma treatment time. (b) Electrophoresis image of HSA samples. Lanes from left to right correspond to protein marker, control sample, and samples treated for 2, 4, 6 and 8 min, respectively

Moreover, despite baseline drifting caused by MS responses, newly appeared bands at 12.0 and 12.8 kDa are observed (Figure 5c). In contrast, variations in the mass spectral range of 100–10,000 *m/z* are not as obvious. The slight increase in signals in the range of less than 2000 m/z in Figure 5b might be caused by excess laser input energy, compared with Figure 5a. In a study by Krewing et al., the cleavage of full-length bovine serum albumin was indirectly proved by UV-absorption measurements at 280 nm and ninhydrin assay [23]. In this work, the MALDI-TOF MS gave direct evidence. Together, destruction of the primary structure is comprehensively confirmed.

Notably, other obvious but unknown vibration bands in FT-IR spectra require further consideration (Figure 2). For instance, the original peak at 1390 cm^{-1} shifts to 1411 cm^{-1} with a treatment time of 8 min, which results in the peak at 1452 cm^{-1} becoming inconspicuous to a shoulder peak, whereas newly appearing strong peaks at 1298 and 945 cm^{-1} are observed after plasma treatment. These new bands are most probably from the protein cleavage products, namely amino acid residues, peptides, or low–molecular weight proteins [35].

3.3 | Secondary structure changes

The amide I band in FTIR spectra is commonly used to analyse the protein secondary structures of α-helix, β-sheet, β-turn, random coil, and aggregated strands [19, 29, 36–38]. Each structure component corresponds to unique hydrogen-bonding pattern and relative steady band positions (Table 2) [29]. The relative content of each component can be obtained from the band area percentage by fitting the amide I band. Figure 6 demonstrates the curve-fitting deconvolution results. The most sensitive secondary structures to plasma are the α-helix and β-sheet. The total content of the α-helix decreases from 45.34% to 14.90% after treatment for 8 min, whereas the β-sheet increases from 20.42% to 40.71% (Table 3). The α-helix content of untreated HSA ranges from 43.7% to 52.3%, as reported by Yuan et al., similar to our results [39]. Moreover, the slight red shift of amide A (~3200 cm^{-1}) and the slight blue shift of amide B (~3076 cm^{-1}) are related to the hydrogen bonding and secondary structure changes [37, 40]. The changing trends of α-helix and β-sheet contents in HSA during plasma treatment revealed in this work are consistent with several reports regarding other proteins [15, 26, 27]. Here, we suggest the amide I band as a possible indicator of plasma-induced protein damage. Hence, the rising shoulder peak between 1620 and 1640 cm^{-1} generated by the β-sheet in the FT-IR spectra may be direct evidence.

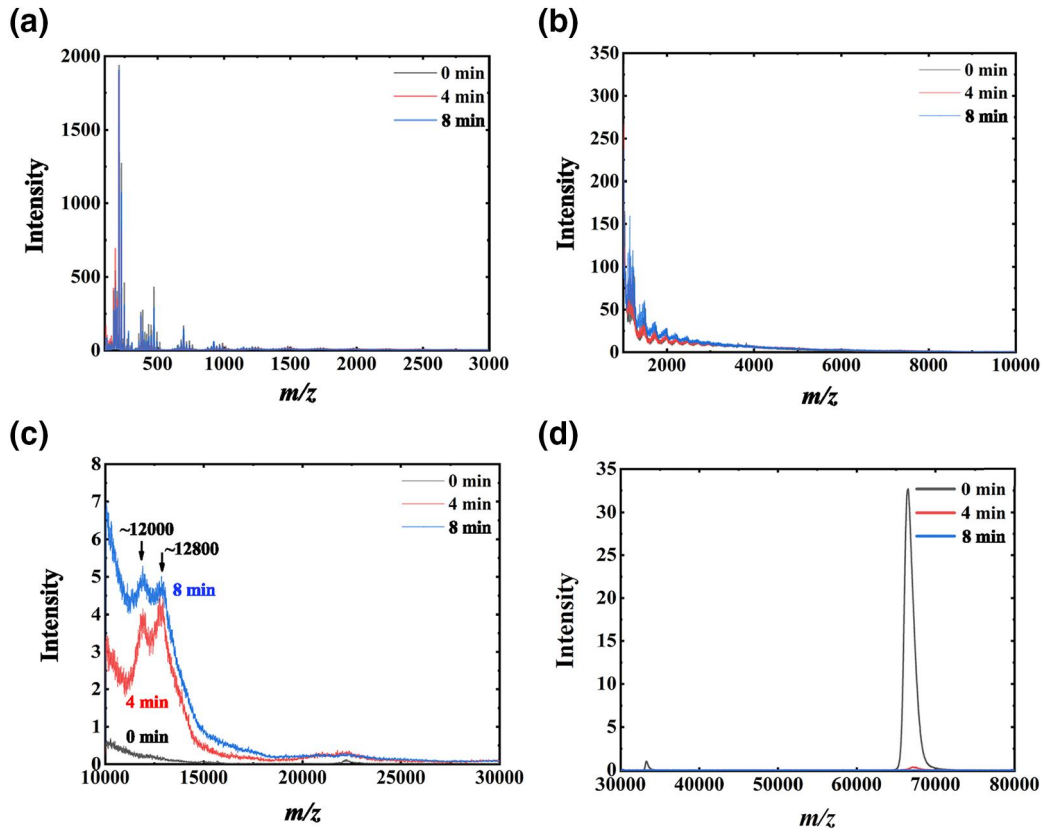

FIGURE 5 Matrix-assisted laser desorption-ionization time of flight mass spectrometry spectra of human serum albumin before and after plasma treatment: (a) 100–3000 (*m/z*); (b) 1000–10,000 (*m/z*); (c) 10,000–30,000 (*m/z*); (d) 30,000–80,000 (*m/z*)

TABLE 2 Assignments of secondary structures in amide I band [15, 19, 29, 30, 36]

Secondary structure	Average band position/cm^{-1}	Band position range/cm^{-1}
Aggregated strands	1615	1600–1618
β-sheet	1633	1618–1640
Random coil	1645	1640–1650
α-Helix	1654	1650–1660
β-Turn	1673, 1681	1660–1689
β-Sheet	1684	1674–1695

3.4 | Plasma agents

Temperatures of ~30°C have almost no effect on proteins [41, 42]. By comparing the experimental spectrum of nitrogen second positive electronic transition $N_2(C^3\Pi_u\text{-}B^3\Pi_g)$ with simulated spectra using Specair software [43], the gas temperature is determined to be around 300 K during 30 min of discharge (Figure S1). Hence, the influence of local heating on the protein can be excluded. In fact, moderate high voltage could avoid sparks and overheating of DBD. Laroussi et al. obtained a similar gas temperature of ≤340K at an applied voltage of 20 kV_{RMS} and 2.2 kHz [44], which is a little higher than 300K at 16kV_p and 1.5 kHz AC in our experiment.

The sample remains in the liquid or moist state even after 8 min of treatment (Figure S2). Accordingly, the influence of UV radiation and electric field on protein damage can be excluded because UV decays quickly in a liquid and low electric field in a sample drop owing to the high relative permittivity of water compared with air [45].

It is well recognized that reactive species can be major contributors to plasma-induced biological response [11]. OH is considered to be the most reactive species in sterilisation and protein damage in a liquid state [12, 46, 47]. The important role

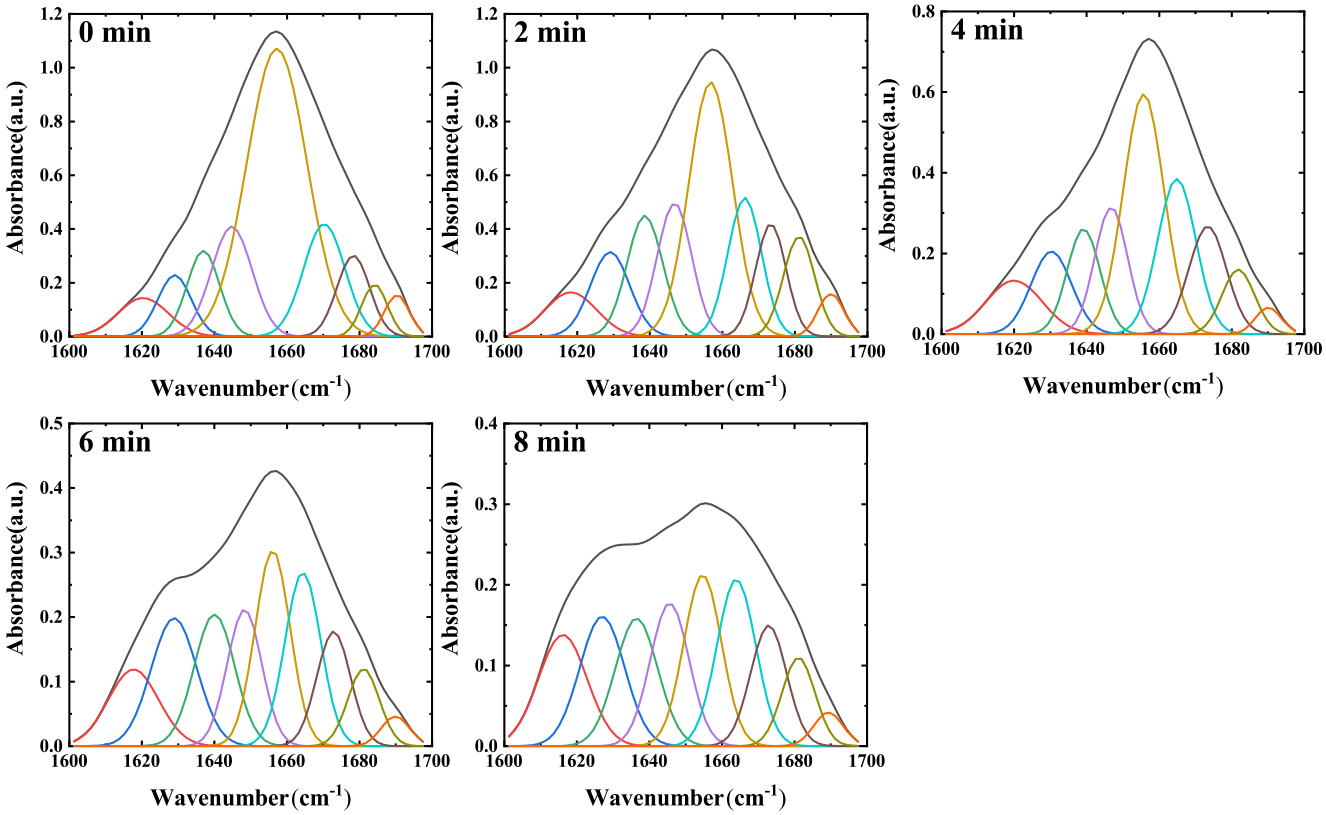

FIGURE 6 Original (top) and deconvoluted (bottom) Fourier transform infrared spectra of amide I band (1700–1600 cm^{-1}) of human serum albumin samples

TABLE 3 Contents of total α-helix and β-sheet of human serum albumin samples with prolonged plasma treatment time

Secondary structures	0 min	2 min	4 min	6 min	8 min
Total α-helix	45.34%	29.31%	26.66%	17.17%	14.90%
Total β-sheet	20.42%	29.09%	28.75%	39.73%	40.71%

of ·OH in the initial cleaving of peptide bonds in protein has been proved [23]. Other species such as O [12, 48], O_3 [49] and $ONOO^-$ [50] may also account for the oxidative damage of protein solutions, and possible synergies among RONS may exacerbate the effects. It requires further studies to clarify what species contribute most to protein damage.

4 | CONCLUSIONS

The comprehensive responses of an HSA solution to air DBD plasma involves oxidative modifications and structural changes. Oxidative responses include carbonylation, side chain modifications, and disulfide bond cross-link, all of which could cause irreversible damage to proteins. Protein primary structure changes (i.e., backbone breakage) and secondary structure changes (mainly a decrease in α-helix and increase in β-sheet) can be also induced by plasma. The role of plasma agents other than RONS has been excluded and requires further investigation into the role of plasma-mediated RONS in protein oxidation and inactivation. Among various methods used in this work, FT-IR spectroscopy is suggested as a feasible and more comprehensive technique to evaluate protein injuries.

ACKNOWLEDGEMENTS

This work was funded by the National Natural Science Foundation of China (52041701), Tsinghua University-Peking Union Medical College Hospital Initiative Scientific Research Programme (20191080604), and Tsinghua University Spring Breeze Fund (2020Z99CFG007).

ORCID

Siqi Peng https://orcid.org/0000-0001-5418-3656

REFERENCES

1. Morfill, G.E., Kong, M.G., Zimmermann, J.L.: Focus on plasma medicine. New J. Phys. 11(11), 115011 (2009)
2. Weltmann, K.D., Woedtke, T.: Plasma medicine - current state of research and medical application. Plasma Phys. Contr. Fusion. 59, 014031 (2017)
3. Li, H.P., et al.: Translational plasma stomatology: applications of cold atmospheric plasmas in dentistry and their extension. High Volt. 2(3), 188–199 (2017)
4. Naidis, G.V., Babaeva, N.Y.: Electric field distributions along helium plasma jets. High Volt. 5(6), 650–653 (2020)

5. Jablonowski, H., von Woedtke, T.: Research on plasma medicine-relevant plasma-liquid interaction: what happened in the past five years? Clin. Plasma Med. 3(2), 42–52 (2015)
6. Laroussi, M., Lu, X., Keidar, M.: Perspective: the physics, diagnostics, and applications of atmospheric pressure low temperature plasma sources used in plasma medicine. J. Appl Phys. 122(2) (2017)
7. Rossi, F., Kylián, O., Hasiwa, M.: Decontamination of surfaces by low pressure plasma discharges. Plasma Process. Polym. 3(6-7), 431–42 (2006)
8. Deng, X.T., Shi, J.J., Kong, M.G.: Protein destruction by a helium atmospheric pressure glow discharge: capability and mechanisms. J. Appl. Phys. 101(7), 074701 (2007)
9. Kylián, O., et al.: Removal of model proteins by means of low-pressure inductively coupled plasma discharge. J. Phys. D Appl. Phys. 41(9), 095201 (2008)
10. Zhang, H., et al.: Roles of membrane protein damage and intracellular protein damage in death of bacteria induced by atmospheric-pressure air discharge plasmas. RSC Adv. 8(38), 21139–21149 (2018)
11. Zhang, L., Wang, H., Luo, H.: Uncovering the inactivation kinetics of Escherichia coli in saline by atmospheric DBD plasma using ATR FT-IR. Plasma Process. Polym. 17(9), 1900197 (2020)
12. Lackmann, J-W., et al.: A dielectric barrier discharge terminally inactivates RNase A by oxidizing sulphur-containing amino acids and breaking structural disulfide bonds. J. Phys. Appl. Phys. 48(49), 494003 (2015)
13. Segat, A., et al.: Atmospheric pressure cold plasma (ACP) treatment of whey protein isolate model solution. Innovat. Food Sci. Emerg. Technol. 29, 247–254 (2015)
14. Yu, X., et al.: Effects of atmospheric pressure plasma jet on the physicochemical, functional, and antioxidant properties of flaxseed protein. J. Food Sci. 85(7), 2010–2019 (2020)
15. Sharifian, A., Soltanizadeh, N., Abbaszadeh, R.: Effects of dielectric barrier discharge plasma on the physicochemical and functional properties of myofibrillar proteins. Innovat. Food Sci. Emerg. Technol. 54, 1–8 (2019)
16. Breusing, N., Grune, T.: Biomarkers of protein oxidation from a chemical, biological and medical point of view. Exp. Gerontol. 45(10), 733–737 (2010)
17. Yu, X., et al.: Effects of atmospheric pressure plasma jet on the physicochemical, functional, and antioxidant properties of flaxseed protein. J. Food Sci, 85(7), 2010–2019 (2020)
18. Zhang, H., et al.: Effects and mechanism of atmospheric-pressure dielectric barrier discharge cold plasmaon lactate dehydrogenase (LDH) enzyme. Sci. Rep. 5(1), 10031 (2015)
19. Dong, S., et al.: Characterisation of physicochemical and structural properties of atmospheric cold plasma (ACP) modified zein. Food Bioprod. Process. 106, 65–74 (2017)
20. Zhou, R., et al.: Interaction of atmospheric-pressure air microplasmas with amino acids as fundamental processes in aqueous solution. PloS One. 11(5), e0155584 (2016)
21. Berlett, B.S., Stadtman, E.R.: Protein oxidation in ageing, disease, and oxidative stress. J. Biol. Chem. 272(33), 20313–20316 (1997)
22. Lackmann1, J-W., et al.: Effects of the effluent of a microscale Atmospheric pressure plasma-jet operated with He/O2 gas on bovine serum albumin. Plasma Med. 3, 115–124 (2013)
23. Krewing, M., Schubert, B., Bandow, J.E.: A dielectric barrier discharge plasma degrades proteins to peptides by cleaving the peptide bond. Plasma Chem. Plasma Process. 40(3), 685–696 (2020)
24. Deng, X.T., et al.: Protein destruction by atmospheric pressure glow discharges. Appl. Phys. Lett. 90(1), 013903 (2007)
25. Fricke, K., et al.: Atmospheric pressure plasma: a high-performance tool for the efficient removal of biofilms. PloS One. 7(8), e42539 (2012)
26. Surowsky, B., et al.: Cold plasma effects on enzyme activity in a model food system. Innovat. Food Sci. Emerg. Technol. 19, 146–152 (2013)
27. Attri, P., et al.: The protective action of osmolytes on the deleterious effects of gamma rays and atmospheric pressure plasma on protein conformational changes. Sci. Rep. 7(1), 8698 (2017)
28. Wang, S., et al.: Interfacial bonding enhancement of the RTV recoating with sandwiched contaminant by plasma jet. High Volt. 4(4), 345–348 (2019)
29. Yang, H., et al.: Obtaining information about protein secondary structures in aqueous solution using Fourier transform IR spectroscopy. Nat Protoc. 10(3), 382–396 (2015)
30. She, Z., et al.: FTIR investigation of the effects of ultra-strong static magnetic field on the secondary structures of protein in bacteria. Infrared Phys. Technol. 52(4), 138–142 (2009)
31. Wehr N.B., Levine R.L.: Quantification of protein carbonylation. Methods Mol. Biol. 965, 265–281 (2013) ed2013
32. Kartaschew, K., et al.: Cold atmospheric-pressure plasma and bacteria: understanding the mode of action using vibrational microspectroscopy. J. Phys. Appl. Phys. 49(37), 374003 (2016)
33. Fabian, H., Mäntele, W.: Infrared spectroscopy of proteins. In: Chalmers, J.M., Griffiths, P.R. (eds.), Handbook of Vibrational Spectroscopy. John Wiley & Sons, Ltd (2006)
34. Compton, S.J., Jones, C.G.: Mechanism of dye response and interference in the Bradford protein assay. Anal. Biochem. 151(2), 369–374 (1985)
35. Wolpert, M., Hellwig, P.: Infrared spectra and molar absorption coefficients of the 20 alpha amino acids in aqueous solutions in the spectral range from 1800 to 500cm^{-1}. Spectrochim Acta. Mol. Biomol. Spectrosc. 64(4), 987–1001 (2006)
36. Carbonaro, M., Nucara, A.: Secondary structure of food proteins by Fourier transform spectroscopy in the mid-infrared region. Amino Acids. 38(3), 679–690 (2010)
37. López-Lorente, Á.I., Mizaikoff, B.: Mid-infrared spectroscopy for protein analysis: potential and challenges. Anal. Bioanal. Chem. 408(11), 2875–2889 (2016)
38. Usoltsev, D., et al.: Systematic FTIR spectroscopy study of the secondary structure changes in human serum albumin under various denaturation conditions. Biomolecules. 9(8), 359 (2019)
39. Yuan, L., et al.: Interaction of mitoxantrone-loaded cholesterol modified pullulan nanoparticles with human serum albumin and effect on drug release. J. Nanomater. 2019, 1–13 (2019)
40. Ryu, S.R., Noda, I., Jung, Y.M.: What is the origin of positional fluctuation of spectral features: true frequency shift or relative intensity changes of two overlapped bands? Appl. Spectrosc. 64(9), 1017–1021 (2010)
41. Fan, M., Cai, W., Shao, X.: Investigating the structural change in protein aqueous solution using temperature-dependent near-infrared spectroscopy and continuous wavelet transform. Appl. Spectrosc. 71(3), 472–479 (2017)
42. Lang, B.E., Cole, K.D.: Unfolding properties of recombinant human serum albumin products are due to bioprocessing steps. Biotechnol. Prog. 31(1), 62–69 (2015)
43. Li, X., et al.: Detection of trace heavy metals using atmospheric pressure glow discharge by optical emission spectra. High Volt. 4(3), 228–233 (2019)
44. Laroussi, M., Leipold, F.: Evaluation of the roles of reactive species, heat, and UV radiation in the inactivation of bacterial cells by air plasmas at atmospheric pressure. Int. J. Mass Spectrom. 233(1-3), 81–6 (2004)
45. Wu, S., et al.: Effect of surface modification of electrodes on charge injection and dielectric characteristics of propylene carbonate. High Volt. 5(1), 15–23 (2020)
46. Hähnel, M., Von Woedtke, T., Weltmann, K-D: Influence of the air humidity on the reduction of Bacillus spores in a defined environment at atmospheric pressure using a dielectric barrier surface discharge. Plasma Process. Polym. 7(3-4), 244–9 (2010)
47. Eto, H., et al.: Low-temperature sterilisation of wrapped materials using flexible sheet-type dielectric barrier discharge. Appl. Phys. Lett. 93(22), 221502 (2008)
48. Lai, W., et al.: Decontamination of biological warfare agents by a microwave plasma torch. Phys. Plasmas. 12(2), 9432 (2005)
49. Pavlovich, M.J., et al.: Ozone correlates with antibacterial effects from indirect air dielectric barrier discharge treatment of water. J. Phys. Appl. Phys. 46(14), 145202 (2013)
50. Lukes, P., et al.: Aqueous-phase chemistry and bactericidal effects from an air discharge plasma in contact with water: evidence for the

formation of peroxynitrite through a pseudo-second-order post-discharge reaction of H_2O_2 and HNO_2. Plasma Sources Sci. Technol. 23(1), 015019 (2014)

SUPPORTING INFORMATION

Additional supporting information may be found online in the Supporting Information section at the end of this article.

How to cite this article: Peng, S., et al.: Oxidative modifications and structural changes of human serum albumin in response to air dielectric barrier discharge plasma. High Volt. 6(5), 813–821 (2021). https://doi.org/10.1049/hve2.12111